SAND2018-1314C

Uncertainty-enabled design of electromagnetic reflectors with integrated shape control

Samiul Haque[a], Laszlo P. Kindrat[b], Li Zhang[c], Vikenty Mikheev[d], Daewa Kim[e], Sijing Liu[f], Jooyeon Chung[g], Mykhailo Kuian[h], Jordan E. Massad[i], Ralph C. Smith[j]

[a,j]North Carolina State University; [b]University of New Hampshire; [c]George Mason University; [d]Kansas State University; [e]University of Houston; [f]Louisiana State University; [g]University of Illinois at Urbana–Champaign; [h]Kent State University; [i]Sandia National Laboratories

ABSTRACT

We implemented a computationally efficient model for a corner-supported, thin, rectangular, orthotropic polyvinylidene fluoride (PVDF) laminate membrane, actuated by a two-dimensional array of segmented electrodes. The laminate can be used as shape-controlled electromagnetic reflector and the model estimates the reflector's shape given an array of control voltages. In this paper, we describe a model to determine the shape of the laminate for a given distribution of control voltages. Then, we investigate the surface shape error and its sensitivity to the model parameters. Subsequently, we analyze the simulated deflection of the actuated bimorph using a Zernike polynomial decomposition. Finally, we provide a probabilistic description of reflector performance using statistical methods to quantify uncertainty. We make design recommendations for nominal parameter values and their tolerances based on optimization under uncertainty using multiple methods.

Keywords: Bimorph membrane, Zernike polynomials, PVDF, Sensitivity analysis, Uncertainty Quantification

1. INTRODUCTION

Thin, flexible membranes made of laminated smart materials can be used as electromagnetic reflectors. Reflectors with controllable shapes may have great potential to be used on space-based scientific telescopes and communication antennae. In this work, polyvinylidene fluoride (PVDF) has been investigated as a flexible piezoelectric material suitable for reflector shape control. A distributed array of actuators is required for shape correction and the ability to maintain paraboloidal geometries is desired. PVDF is a polymer exhibiting strong piezoelectricity. It is relatively low cost and is typically manufactured as thin films. To achieve shape control with piezoelectric laminate actuators, it is necessary to develop models that predict displacements given field inputs. Mathematical models of a PVDF laminate with segmented actuators have been proposed.[1,2] However, the sensitivity of reflector performance to design parameter variations and the impact of uncertainty in those parameters have not been addressed. As the design parameters and voltage distribution have their own tolerances, it is logical to assume that the variation in these parameters will affect shape error.

In this work, we develop a computationally-efficient implementation of a model originally proposed by Massad and Sumali[1] that simulates deflection of the laminate. Then, we quantify shape error and perform a sensitivity analysis of its physical parameters. Subsequently, we report the important parameters of the model. Via uncertainty propagation, we also show that the shape error has a bimodal distribution in the presence of parameter uncertainty. Finally, we demonstrate that optimization under uncertainty can be performed to improve shape error in the presence of design uncertainty.

Further author information: (Send correspondence to R.C. Smith)
S. Haque.: E-mail: shaque2@ncsu.edu, L.P. Kindrat: E-mail: laszlokindrat@gmail.com, L. Zhang: E-mail: zhang18@masonlive.gmu.edu, V. Mikheev: E-mail: vikentym@ksu.edu, D. Kim: E-mail: daewakim@math.uh.edu, S. Liu: E-mail: sliu42@lsu.edu, J. Chung.: E-mail: jchung50@illinois.edu, M. Kuian: E-mail: mkuian@kent.edu, J. Massad: E-mail: jemassa@sandia.gov, R.C. Smith: E-mail: rsmith@ncsu.edu

2. PROBLEM DESCRIPTION

The smart laminate is a membrane of rectangular shape with area $a \times b$, where a and b are measured in the x and y directions, respectively. The laminate simulated here has three layers: the top PVDF and bottom PVDF layer are orthotropic and each have thickness h_p The laminate x-axis is oriented along the polymer stretching direction of the top PVDF layer. The bottom PVDF layer is oriented so that the stretching direction is along the laminate y-axis, i.e. the bottom PVDF layer is oriented 90° with respect to the top PVDF layer. Between the two PVDF layers, the middle layer is a bonding layer made of an isotropic material, such as epoxy, with thickness h_e. Hence, the total laminate thickness h is

$$h = 2h_p + h_e.$$

The membrane is equipped with electrode layers, which we assume to be of negligible thickness for this analysis. On one side, a single grounded electrode covers the membrane, while on the opposite side, the membrane has segmented electrodes, whose voltage can be controlled individually. We only consider rectangular electrodes with sides parallel to the x and y-axes. We define x_{1_i} and x_{2_i} as the x-coordinates of the right and left side of the i-th segment, and similarly, y_{1_i} and y_{2_i} are the y-coordinates of the bottom and top of i-th segment

$$\{(x, y) \mid x_{1_i} \leq x \leq x_{2_i},\ y_{1_i} \leq y \leq y_{2_i}\}. \tag{1}$$

Aside from the above restrictions, the number and distribution of electrodes is not limited.

A voltage V_i is applied to the i-th electrode on the top, while the bottom electrode is grounded. On electrode i, this voltage results in an electric field $E_i = V_i/h$ that is assumed uniform through the cross section of the laminate. The electric field E_i does not change signs throughout the whole thickness h. When the top PVDF layer expands as a result of E_i, the bottom PVDF layer contracts, and vice versa, thereby creating bimorph, out-of-plane bending. We employ an energy-based model that predicts the deflection of a laminate with orthotropic active layers given a distribution of electrode voltages. The fundamental principle we employ is that the laminate responds to a voltage distribution in such a way that the deformation potential energy is minimized.

We implement an efficient model that allows us to quickly calculate the laminate shape for an arbitrary electrode pattern and voltage distribution and use model-based optimization techniques. The model output allows us to compare the numerically calculated surface shape to an ideal shape. We compare the deflection w calculated by the model to a reference paraboloid as it has been shown that uniform actuation results in a paraboloidal shape of deflection.[1]

2.1 Mathematical model

We implemented a Ritz-based model[3] that can calculate the deflection of the orthotropic laminate for a given distribution of segment voltages. The deflection of a corner-supported plate is approximated by the finite expansion

$$w(x, y) \approx \sum_{j=1}^{j_{max}} a_j \cos\left(m_j \pi \frac{x}{a}\right) \sin\left(n_j \pi \frac{y}{b}\right) + b_j \cos\left(m_j \pi \frac{y}{b}\right) \sin\left(n_j \pi \frac{x}{a}\right), \tag{2}$$

where the basis functions satisfy the zero deflection condition at the corners,[4] and m_j and n_j are non-negative and positive integers, respectively.[2] The model yields the linear matrix equation

$$\begin{bmatrix} \mathbf{2A} & \mathbf{C} \\ \mathbf{C} & \mathbf{2B} \end{bmatrix} \begin{bmatrix} \mathbf{a} \\ \mathbf{b} \end{bmatrix} = \begin{bmatrix} \mathbf{A^{act}} \\ \mathbf{B^{act}} \end{bmatrix} \mathbf{V}, \tag{3}$$

where $\mathbf{A}$, $\mathbf{B}$, $\mathbf{C}$, $\mathbf{A^{act}}$ and $\mathbf{B^{act}}$ are nonlinear functions of the design parameters, such that $\mathbf{C} \in \mathbb{R}^{\mathbf{j_{max}} \times \mathbf{j_{max}}}$ is the matrix of elements C_{jk}, $\mathbf{A}, \mathbf{B} \in \mathbb{R}^{\mathbf{j_{max}} \times \mathbf{j_{max}}}$ are diagonal matrices containing A_j and B_j respectively, and $\mathbf{a}, \mathbf{b} \in \mathbb{R}^{\mathbf{j_{max}}}$ are vectors of the Reed coefficients,[4] a_j and b_j. The matrices $\mathbf{A^{act}}$, $\mathbf{B^{act}} \in \mathbb{R}^{\mathbf{j_{max}} \times \mathbf{i_{max}}}$ contain $\frac{D_{act}}{h} A_j^{act_i}$ and $\frac{D_{act}}{h} B_j^{act_i}$, respectively, and $\mathbf{V} \in \mathbb{R}^{\mathbf{i_{max}}}$ is the voltage distribution with i-th component V_i.

The entries of the parameter matrices are

$$A_j = \frac{\pi^4}{4a^3b^3}\left[D_{11}b^4m_j^4 + 2(D_{12}+2D_{66})a^2b^2m_j^2n_j^2 + \gamma_j D_{22}a^4n_j^4\right], \tag{4}$$

$$B_j = \frac{\pi^4}{4a^3b^3}\left[\gamma_j D_{11}b^4n_j^4 + 2(D_{12}+2D_{66})a^2b^2m_j^2n_j^2 + D_{22}a^4m_j^4\right]. \tag{5}$$

where the orthotropic plate stiffness constants have the form

$$D_{11} = D_{22} = \frac{Y_e h_e^3}{12(1-\nu_e^2)} + \frac{(Y_{11}+Y_{22})h_p}{12(1-\nu_{12}\nu_{21})}(4h_p^2 + 6h_p h_e + 3h_e^2), \tag{6}$$

$$D_{12} = \frac{\nu_e Y_e h_e^3}{12(1-\nu_e^2)} + \frac{\nu_{12}Y_{22}h_p}{6(1-\nu_{12}\nu_{21})}(4h_p^2 + 6h_p h_e + 3h_e^2), \tag{7}$$

$$D_{66} = \frac{Y_e h_e^3}{24(1+\nu_e)} + \frac{G_{12}h_p}{6}(4h_p^2 + 6h_p h_e + 3h_e^2), \tag{8}$$

For $m_j \neq n_k$ and $m_k \neq n_j$, the C_{jk} coefficient has the form

$$C_{jk} = \frac{2\pi^2}{a^3b^3}\frac{\chi_{jk}n_j n_k}{(m_j^2-n_k^2)(m_k^2-n_j^2)}\left[D_{11}b^4m_j^2n_k^2 + (D_{12}+4D_{66})a^2b^2m_j^2m_k^2 + D_{12}a^2b^2n_j^2n_k^2 + D_{22}a^4m_k^2n_j^2\right], \tag{9}$$

otherwise $C_{jk} = 0$. The orthogonality parameters are

$$\gamma_j = \begin{cases} 2, & \text{if } m_j = 0, \\ 1, & \text{otherwise,} \end{cases} \qquad \text{and} \qquad \chi_{jk} = \left[(-1)^{m_j+n_k} - 1\right]\left[(-1)^{n_j+m_k} - 1\right]. \tag{10}$$

The actuation constants are calculated over the i-th actuator region $(x_{1_i}, x_{2_i}) \times (y_{1_i}, y_{2_i})$. For nonzero m_j,

$$A_j^{act_i} = 4\left(\frac{an_j}{bm_j} + \frac{bm_j}{an_j}\right)\sin\left(m_j\pi\frac{x_{2_i}-x_{1_i}}{2a}\right)\cos\left(m_j\pi\frac{x_{2_i}+x_{1_i}}{2a}\right)\sin\left(n_j\pi\frac{y_{2_i}-y_{1_i}}{2b}\right)\sin\left(n_j\pi\frac{y_{2_i}+y_{1_i}}{2b}\right), \tag{11}$$

$$B_j^{act_i} = 4\left(\frac{am_j}{bn_j} + \frac{bn_j}{am_j}\right)\sin\left(n_j\pi\frac{x_{2_i}-x_{1_i}}{2a}\right)\sin\left(n_j\pi\frac{x_{2_i}+x_{1_i}}{2a}\right)\sin\left(m_j\pi\frac{y_{2_i}-y_{1_i}}{2b}\right)\cos\left(m_j\pi\frac{y_{2_i}+y_{1_i}}{2b}\right). \tag{12}$$

For $m_j = 0$,

$$A_j^{act_i} = 2\pi n_j\frac{(x_{2_i}-x_{1_i})}{b}\sin\left(n_j\pi\frac{y_{2_i}-y_{1_i}}{2b}\right)\sin\left(n_j\pi\frac{y_{2_i}+y_{1_i}}{2b}\right), \tag{13}$$

$$B_j^{act_i} = 2\pi n_j\frac{(y_{2_i}-y_{1_i})}{b}\sin\left(n_j\pi\frac{x_{2_i}-x_{1_i}}{2a}\right)\sin\left(n_j\pi\frac{x_{2_i}+x_{1_i}}{2b}\right). \tag{14}$$

Solving (3), the deflection of the laminate $w(x, y)$ is calculated using formula (2). Throughout our simulations, we used $j_{max} = 32$ basis functions. Whereas the system is linear in the coefficients $\mathbf{a}$ and $\mathbf{b}$, the matrices on the left and right hand side of (3) are nonlinear functions of the physical parameters, and hence the investigation of the model as a function of these parameters is a non-trivial problem. The described model was validated by experiments and finite element analysis.[1] The nominal values and tolerances for the physical and geometric parameters are listed in Table 1. Throughout the paper we assumed uniformly spaced electrodes, for which simulation results can be seen in Figure 1 for various voltage distributions. The model has been extended to simulate unevenly distributed, rectangular electrodes as well to better accommodate variation and uncertainty in the electrode dimensions.

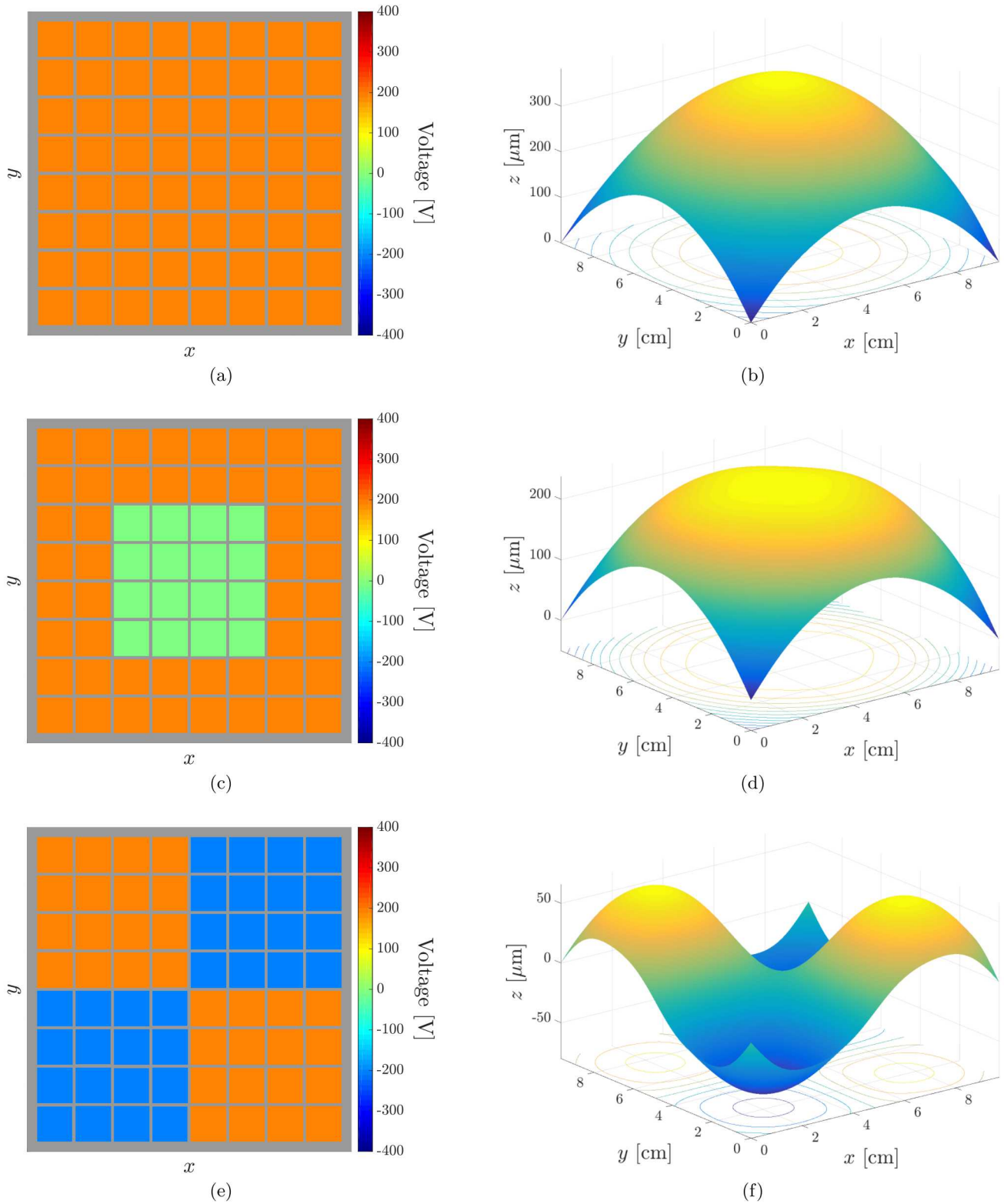

Figure 1: Electrode patterns and the simulated membrane shapes for various voltage distributions. The gray area on the membrane is not covered by electrodes.

Parameter	Description	Nominal value	Tolerance
Physical Parameters			
Y_{11}	PVDF Young's modulus	2.7 GPa	±35%
Y_{22}	PVDF Young's modulus	2.5 GPa	±35%
G_{12}	PVDF shear modulus	0.935 GPa	±5%
Y_e	Epoxy Young's modulus	1.03 GPa	±50%
ν_{12}	PVDF Poisson ratio	0.326	±5%
ν_e	Epoxy Poisson ratio	0.35	±10%
d_{31}	Piezoeletric strain constant	23×10^{-12} m/V	±25%
d_{32}	Piezoeletric strain constant	2.3×10^{-12} m/V	±25%
Geometric Parameters			
a, b	Laminate length, width	97 mm	±5%
h_p	PVDF thickness	52 μm	±20%
h_e	Epoxy thickness	30 μm	±100%
Bor	Non active PVDF border	5 mm	±10%
Sep	Separation between the electrodes	1 mm	±5%
Other Parameter			
V	Voltage	Between ±200 V	±5%

Table 1: Model parameters and their nominal values used in this analysis.[3] The range of uncertainty of each parameter is indicated in the Tolerance column.

2.2 Implementation of the model

The implementation of the model, as well as the consequent simulations and analyses, were done in MATLAB. In each simulation, the values of simulation parameters are first determined, including the physical and geometric parameters, electrode voltages, and modeling parameters (e.g. j_{max}). Then the matrices governing (3) are calculated and the system is solved using MATLAB's linear solvers. Finally, the membrane deflection (2) is evaluated on a chosen grid. The scalar responses used for statistical analysis (see Sections 3.1–3.2) can be calculated from the membrane deflection w.

The linear model described above is computationally efficient when calculating the coefficients **a** and **b**: our investigation showed that even for moderate grid sizes – e.g. 256×256 – the evaluation of the deflection function w could take 100 times longer than solving the linear model. To mitigate this effect, our implementation for the evaluation of w precalculates the shape functions in (2) on the desired grid, hence large batches of simulations can be efficiently performed without the need for reevaluating the shape functions. In rest of the paper, we consider an 8×8 uniform electrode grid and uniform voltage distribution.

3. METHODS

3.1 Relative shape error

We compared the deflection calculated by the model to a reference paraboloid w_{ref}. We used the root square error to quantify the relative shape error; namely,

$$RSE = \frac{\|w - w_{ref}\|_2}{\|w_{ref}\|_2}, \tag{15}$$

where w and w_{ref} are the deflections at each discretization point on the membrane surface. Firstly, we parameterized a reference paraboloid that is symmetrical around the z-axis with zero height at the corners (x_1, y_1), (x_1, y_2), (x_2, y_1), and (x_2, y_2) of the rectangular domain, with center at $(0, 0)$ and with the peak height w_{peak}. The equation of a symmetric paraboloid is given as

$$w_{ref} = w_{ref}(x, y) = k(x^2 + y^2) + j(x + y) + h_p. \tag{16}$$

We also obtained two equations from the corner-supported condition:

$$0 = k(x_1^2 + y_1^2) + j(x_1 + y_1) + h_p, \qquad 0 = k(x_2^2 + y_2^2) + j(x_2 + y_2) + h_p. \tag{17}$$

Solving the system (17) for the unknown coefficient k in terms of h_p yielded

$$k = h_p \left[\frac{x_2 + y_2 - x_1 - y_1}{(x_1 + y_1)(x_2^2 + y_2^2) - (x_2 + y_2)(x_1^2 + y_1^2)} \right].$$

3.2 Zernike polynomial decomposition

Examining the deviation of membrane shapes from a perfect paraboloid can yield some understanding of the error. However, decomposing the achieved shape into characteristic shapes can reveal more information about the nature of shape error. A common method used in optics is decomposition into Zernike polynomial basis,[5] where the even and odd Zernike polynomials are respectively given by the formulas

$$Z_n^m(\rho, \varphi) = R_n^m(\rho)\, \cos(m\, \varphi), \qquad Z_n^{-m}(\rho, \varphi) = R_n^m(\rho)\, \sin(m\, \varphi). \tag{18}$$

Here m and n are natural numbers with $n \geq m$, φ is the azimuthal angle, ρ is the radial distance $0 \leq \rho \leq 1$, and R_{mn} are the radial polynomials defined as

$$R_n^m(\rho) = \sum_{k=0}^{\frac{n-m}{2}} \frac{(-1)^k\, (n-k)!}{k!\, \left(\frac{n+m}{2} - k\right)!\, \left(\frac{n-m}{2} - k\right)!}\, \rho^{n-2\,k}$$

for $(n - m)$ even, and are zeros for $(n - m)$ odd. Zernike polinomials are orthogonal on the unit disk, and $|Z_n^m(\rho, \varphi)| \leq 1$. For our analysis, we chose the first twelve 12 Zernike polynomials, of which some are shown in Figure 2. Then $w^{fit}(r, \theta) = \sum_{p=1}^{12} c_p z_p(r, \theta)$ is an approximation of the simulated membrane deflection w. To find $c = [c_1, c_3, ..., c_{12}]$, we used a least squares approximation.

To use Zernike decomposition, we needed to map our rectangular domain onto the unit disk. There are several ways of doing this, but unlike Sumali et al.,[1] we transformed a rectangular domain to a similar rectangle using the rule

$$x'_{norm} = \frac{2}{\sqrt{\Delta x^2 + \Delta y^2}}(x - \Delta x/2), \qquad y'_{norm} = \frac{2}{\sqrt{\Delta x^2 + \Delta y^2}}(y - \Delta y/2). \tag{19}$$

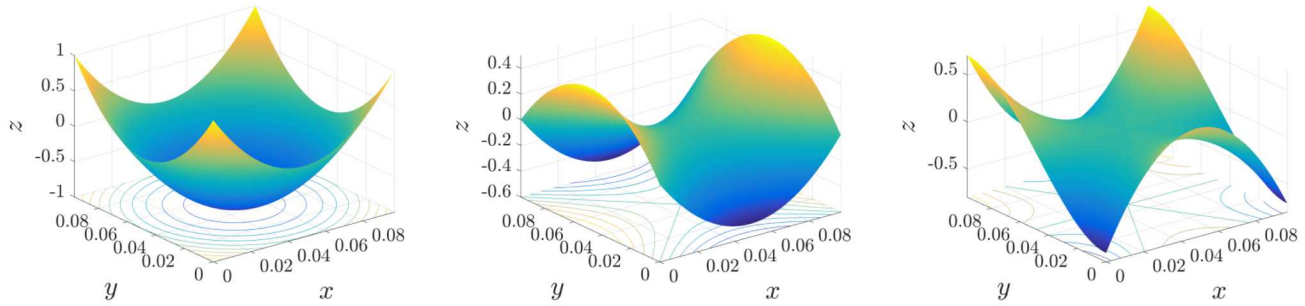

(a) $z_5 = 2r^2 - 1$ (b) $z_6 = r^2 \cos(2\theta)$ (c) $z_7 = r^3 \sin(3\theta)$

Figure 2: Plots of select Zernike polynomials.

3.3 Sensitivity analysis

For any problem of uncertainty quantification and parameter estimation, it is important to ascertain the sensitive and insensitive parameters. One of our main focuses in this work was to identify the sensitive and significant parameters, so that the manufacturer can consider improving the tolerances of these physical or geometric

parameters. We defined our quantity of interest (QoI) to be the relative shape error (RSE) in (2). To identify the significant and influential parameters of the model, we performed sensitivity analysis. We defined the tolerance for each parameter in Table 1 based on product specifications and subject matter expertise. We computed sensitivity of RSE to each parameter by performing one-at-a-time (OAT) variable sweep over a uniform interval, by performing an multi-variable Latin Hypercube Sampling (LHS) over the parameter space for 14 parameters, and by calculating Partial Rank Correlation Coefficient (PRCC).[6] We used these three methods to generate a ranking of parameters based on their influence on model response.[7]

3.4 Optimization under uncertainty

Optimization under uncertainty is an inverse problem. We have performed two different types of optimization. In one, we estimated the optimum mean value of the parameters under a specified tolerance; in the other, we searched for improved tolerance value for each of the design parameters. We briefly describe these two approaches below.

3.4.1 Mean value optimization

In this approach we maintained all the variations in the parameter and searched for a new mean or nominal values that result in improved RSE distribution. We chose to minimize the value of an arbitrarily chosen RSE quantile. MATLAB's `fminsearch` method was used to estimate the optimum values for six most significant parameters reported. The mean values and tolerances of other non-influential parameters were left unaltered.

3.4.2 Tolerance optimization

We also searched for improved upper and lower bounds for parameter variations that yield a distribution with lower relative shape error despite input uncertainty. This can be considered as a combination of design and process optimization. Differential Evolution (DE)[8,9] is an effective evolution algorithm to find approximate solutions to complex problems with minimal assumptions on the parameters. A typical Differential Evolution algorithm starts with a set of initialization parameter values. For practical purposes, the difference between the optimized upper and lower bounds cannot be too small, as we need to accommodate some uncertainty resulting from the manufacturing process. We searched for a set of lower and upper bounds within the current boundaries, so we modified the original DE to Constrained Differential Evolution (CDE) by adjusting the objective function. The CDE algorithm takes the input of a combined vector of lower and upper bounds. We wish to evaluate the estimated quantile value q for each iteration of CDE. Ideally q should be a value between 85% and 95% to accommodate outliers. However, because of the generally expensive computation of DE, we decided to take a small sample out of each interval and take the maximum value of the RSE as the sampling distribution is expected to have a shorter tail compared to the true distribution. Therefore, the objective function evaluated the maximum of RSE from the sampled parameters within the range. Note that during the iterations, the boundary candidates could fall out of range. Hence a large penalty was added to the candidate which exceeds any set bounds, and the order of lower and upper bounds were adjusted for the cases where they became distorted. The rest of CDE followed the standard DE procedure after initialization with objective function, repeat mutation, recombination and selection through our objective function.

4. RESULTS

4.1 Sensitivity analysis

Figure 3 represents the result from OAT sensitivity analysis when we change the mean value of one variable and enforce other variables to remain at their nominal values. This figure shows that when the uncertainties of all other parameters are absent, Bor, a, b, G_{12}, and Y_{22} are the most sensitive parameters. The slopes of the lines represents the sensitivity of each of the parameters.

Figure 4 shows the change in RSE against four parameters when all parameters were allowed to have uncertainties specified in Table 4. We used a LHS scheme to generate 10000 samples in the 14-dimensional parameter space. On the scatter plots of the parameter value against RSE, we fitted a straight line and used the slopes of these lines to rank the parameters according to their influence on model response. We have conducted these two analyses for all 14 parameters of our model and also calculated the sensitivity of the uniform voltage input.

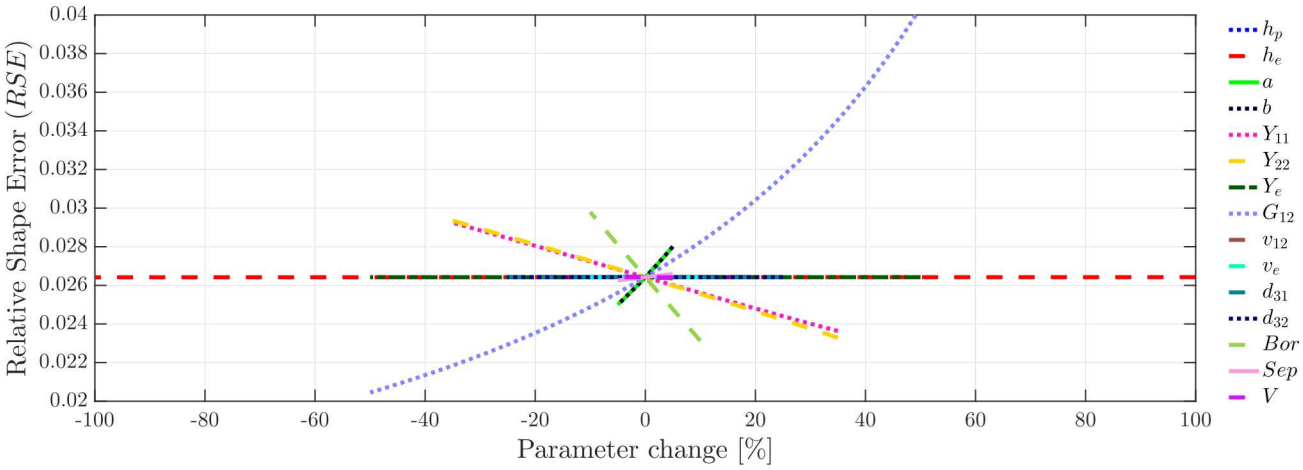

Figure 3: Sensitivity analysis for different parameters, evaluated one at a time. Each parameter is varied independently while fixing others to their nominal values. The horizontal axis shows percentage change of the parameter value from its nominal value; the vertical axes is the amount of relative shape error.

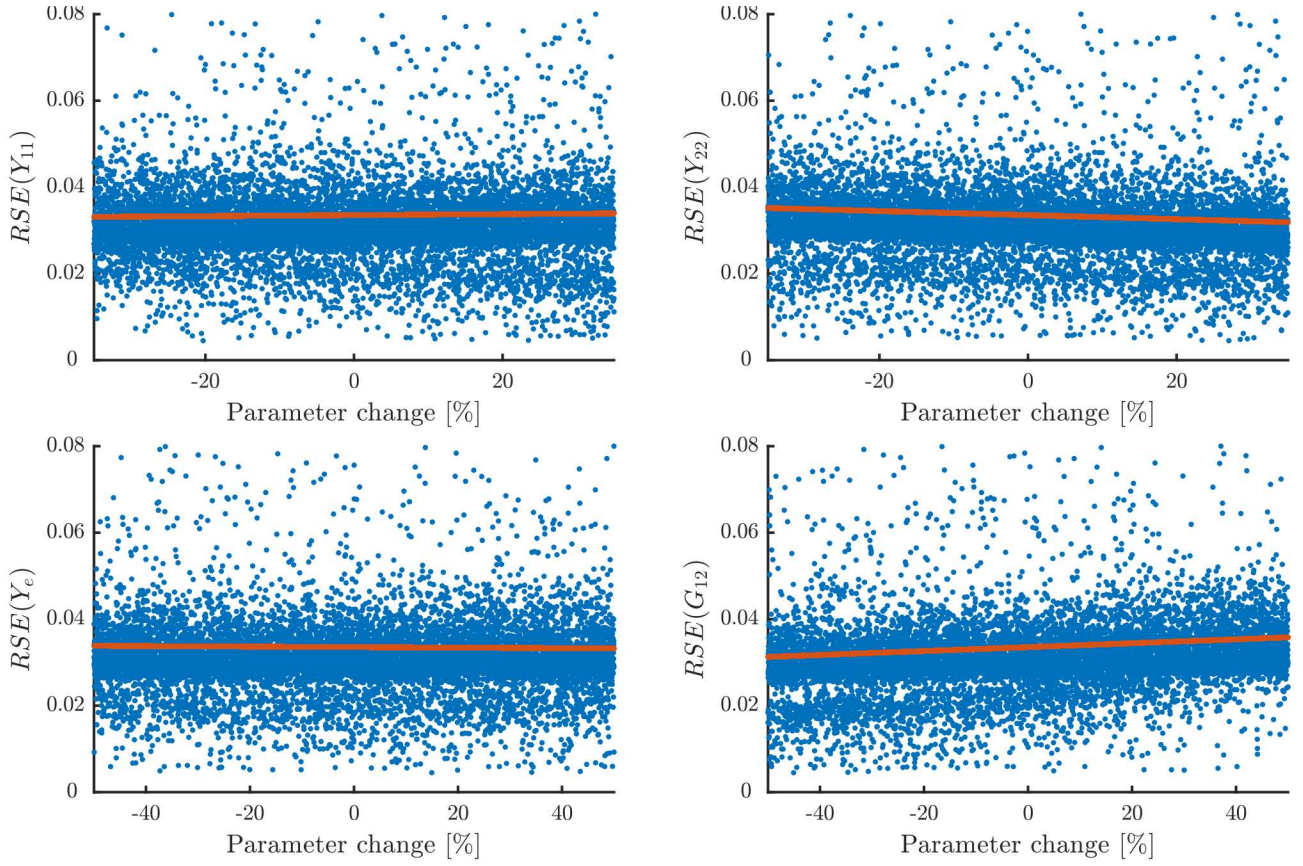

Figure 4: LHS sensitivity analysis for parameters Y_{11}, Y_{22}, Y_e, G_{12}. RSE is plotted against parameter change, while all parameters are allowed to vary within their uncertainty ranges. A line is fitted to elucidate the change in RSE with changing parameter value.

Parameter	Sensitivity rank (OAT)	LHS sensitivity rank (Latin Hypercube)	Significance rank	PRCC	PRCC rank
h_p	9	11	7	0.0121	11
h_e	10	13	7	0.0110	12
a	2	1	5	0.3866	2
b	2	1	5	-0.4387	1
Y_{11}	5	10	3	-0.0307	6
Y_{22}	4	5	2	0.2411	4
Y_e	11	12	7	0.0063	13
G_{12}	3	6	1	-0.2712	3
ν_{12}	7	2	7	0.0277	7
ν_e	8	7	7	-0.0153	10
D_{31}	13	8	7	-0.0168	9
D_{32}	12	9	7	0.0234	8
Bor	1	3	4	0.1042	5
Sep	6	4	6	0.0017	14

Table 2: Summary of OAT, LHS, and PRCC sensitivity analysis.

Table 2 represents the summary of the sensitivity analysis. We observe that, even though some parameters are very sensitive, they do not have significant effect on the response (RSE) as their range of variation (tolerance) is very limited. Dimensions a and b have the highest sensitivity score, but as they vary by only 5%, their significance rank is less than that of G_{12} or Y_{22}. Finally, to further support our findings from the LHS, we calculated the Partial Rank Correlation Coefficients (PRCC).[6] The PRCC values are also given in Table 2 and our visual observations and ranking using the slopes were consistent with the PRCC values.

4.2 Distribution of shape error

We calculated the distribution of shape error by propagating the uncertainty of input parameters to the output response. We generated 10000 samples of all the 14 parameters by LHS from uniform distributions having the mean values and bounds as shown in Table 4. We evaluated the RSE for each of these parameter vectors. We found that the shape error has a bimodal distribution that can be seen in Figure 5. The "dip" between the two modes is around 0.0245 as indicated by the vertical red dashed line in Figure 5.

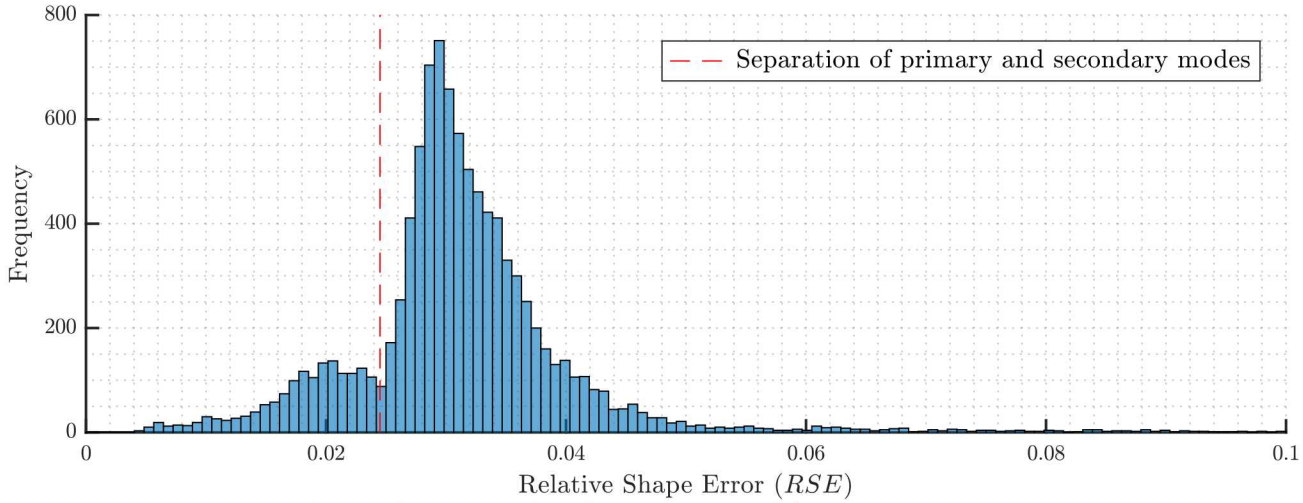

Figure 5: Relative shape error distribution generated from uncertainty propagation.

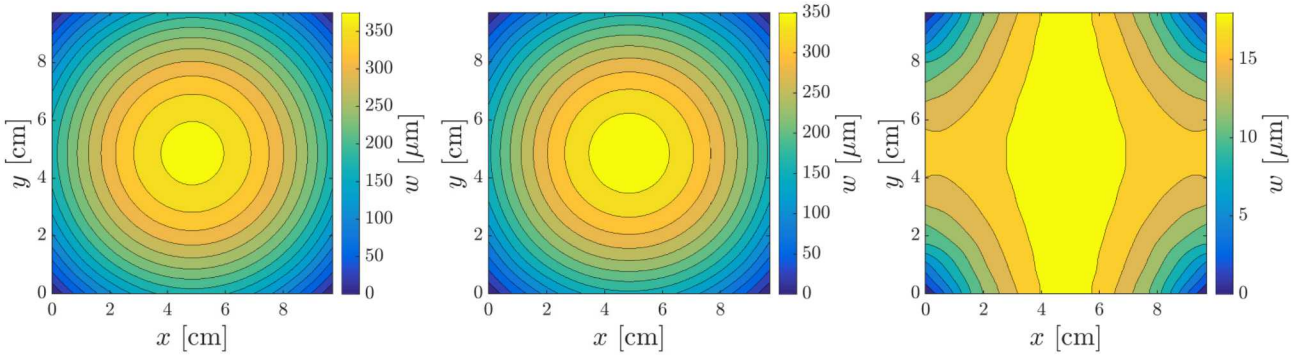

(a) Average shape of secondary mode (b) Average shape of primary mode (c) Difference of the average shapes.

Figure 6: Average membrane shapes and their difference.

We examined the qualitative and quantitative differences and similarities between the primary and secondary modes of the shape error distribution. After separating the two modes of shape error distribution at 0.0245, we averaged the **a** and **b** coefficients within each mode and calculated the corresponding membrane shape w. As it can be seen in Figure 6, the average shapes corresponding to the primary and secondary modes differ significantly in an asymmetric manner. We calculated the Zernike decomposition of the simulation results as described in Section 3.2, to quantify this difference. The membrane deflections only had z_1, z_5, and z_6 components that were non-zero, of which z_6 (astigmatism) is responsible for the asymmetry seen in Figures 6. The histogram of the z_6 coefficient in Figure 7 shows a clear difference between the two modes; the primary mode itself is bimodal, while the secondary mode of c_6 is severely skewed.

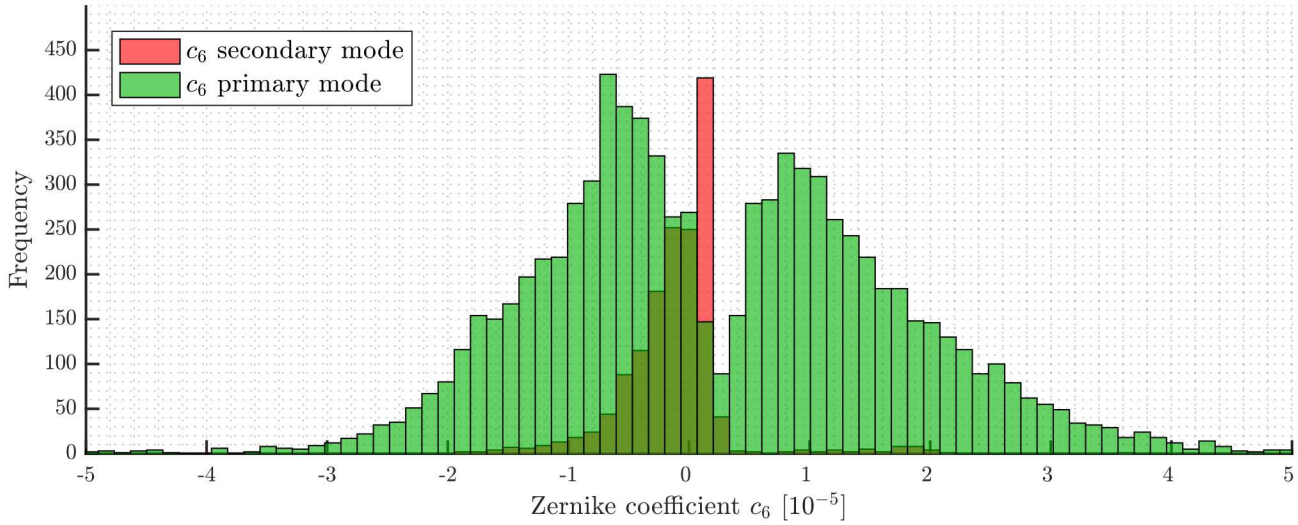

Figure 7: Distribution of coefficients of the z_6 Zernike polynomial for the primary and secondary modes.

We also investigated the distributions of the parameter values in the two modes to find the parameters potentially responsible for the bimodality. Figure 8 shows that the distributions of Y_{11} and G_{12} (which were found to be significant parameters in the sensitivity analysis above) differ significantly between the two modes. This indicates that Y_{11} and G_{12} may have important roles in the observed bimodality of the shape error distribution.

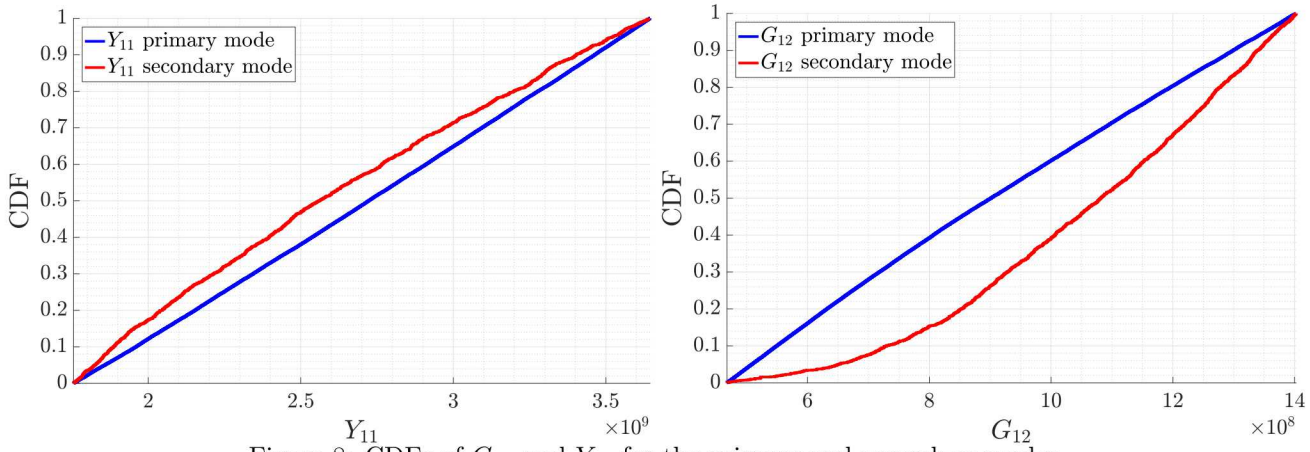

Figure 8: CDFs of G_{12} and Y_{11} for the primary and secondary modes.

4.3 Optimization under uncertainty

We optimized the six most sensitive parameters to get a better *RSE* distribution under specified uncertainty and found a parameter set that produced improved *RSE* distributions compared to that of the nominal values. Figure 9 shows the cumulative distribution function (CDF) of *RSE* with nominal parameter values as given in Table 1, and the CDF of *RSE* with optimized values given in Table 3. The CDFs were obtained by perturbing the model with two different sets of 10000 random samples. This result demonstrates that even a simple algorithm like `fminsearch` can find improved values for the design parameters of the reflectors. The mean values of the six parameters before and after the optimization are listed in Table 3.

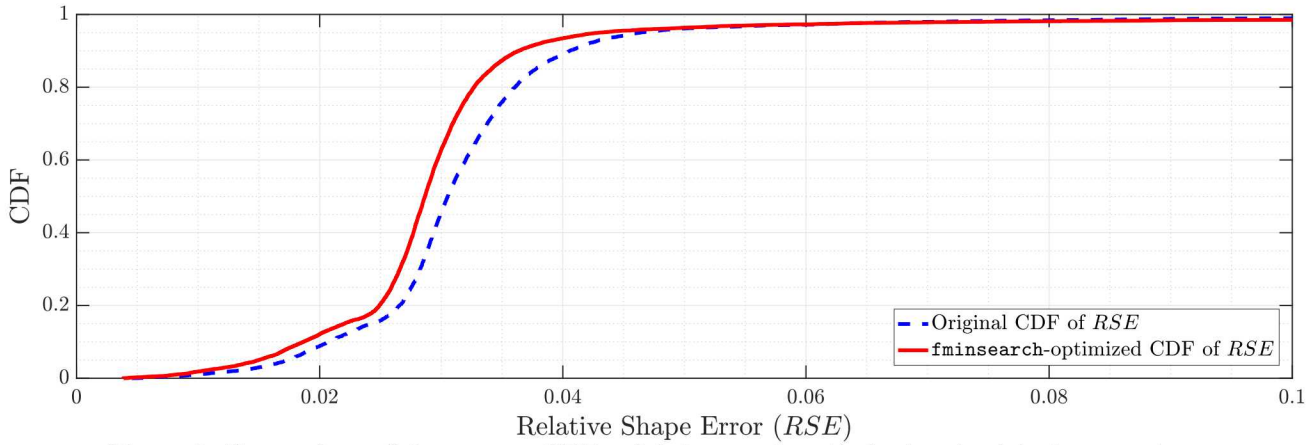

Figure 9: Comparison of shape error CDFs of `fminsearch`-optimized and original parameters.

Parameter	Original value	Optimized value	Unit
a	97	96.4	mm
b	97	97.7	mm
Y_{11}	2.7	5.9359	GPa
Y_{22}	2.5	1.4729	GPa
G_{12}	0.935	1.1106	GPa
Bor	5	3.2	mm

Table 3: Optimization results using MATLAB's `fminsearch`.

There is a difference between the optimized width and length of the laminate. Further investigation is warranted to explain this phenomenon.

4.4 Tolerance optimization

We generated 10000 random LHS samples from the original bounds and the optimized bounds obtained by CDE respectively, then computed the RSE distribution for both set of samples. Figure 10 shows the CDF of the two set of errors produced by two types of uncertainty bounds on the parameters (original tolerance bounds and CDE-optimized tolerance bounds). The plot indicates that our method improves the error in most quantiles of the distribution, and the magnitude of improvement is especially significant between quantiles 30% to 86%. Table 4 shows the original and optimized parameter values and tolerance ranges. The table indicates that tighter tolerances on some parameters (e.g. G_{12}, and Y_{11}) will result in better error minimization.

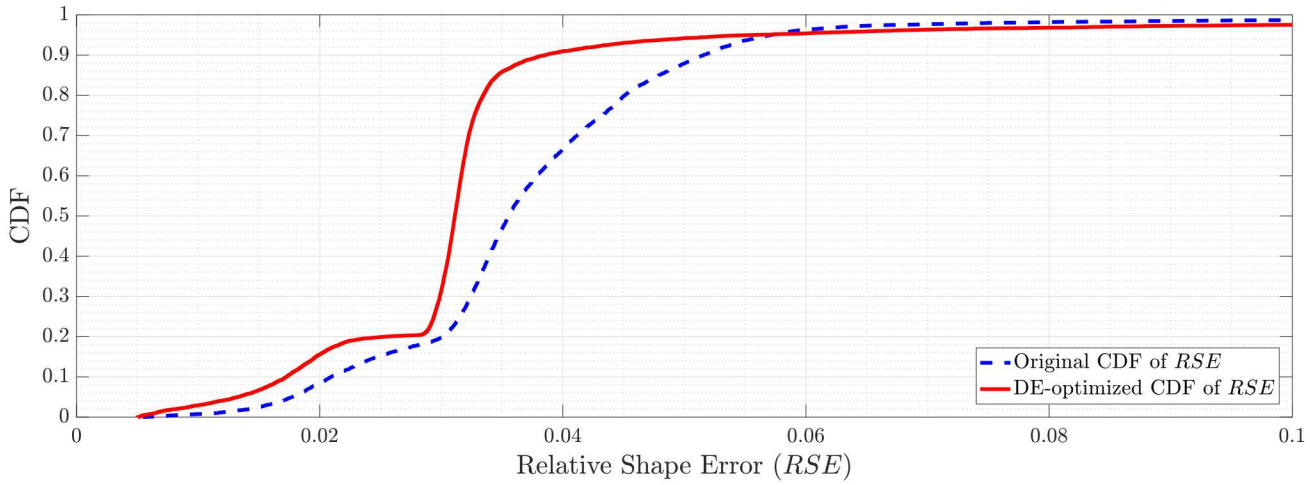

Figure 10: Comparison of shape error CDFs of Differential Evolution-optimized and original parameters.

Parameter	**Original nominal values**	**Original tolerance (±%)**	**New nominal values**	**New tolerance (±%)**	**Unit**
h_p	52	20	44.47	6.9	μm
h_e	30	100	14.38	100	μm
a	97	5	95.68	1.24	mm
b	97	5	97.62	1.06	mm
Y_{11}	2.7	35	3.15	15.39	GPa
Y_{22}	2.5	35	2.367	31.35	GPa
Y_e	1.03	50	0.866	2.48	GPa
G_{12}	0.935	50	1.135	20.36	GPa
ν_{12}	0.3260	5	0.3260	5	GPa
ν_e	0.35	10	0.335	0.32	-
d_{31}	23	25	25.78	11.02	m/V
d_{32}	2.3	25	2.3	25	m/V
Bor	0.005	10	0.00468	3.89	m
Sep	0.001	5	0.001	4.76	m
V	200	5	199.76	2.92	V

Table 4: Parameter values and tolerance ranges after optimizing with Constrained Differential Evolution

5. CONCLUSION

In this work, we have implemented a model for a corner supported PVDF laminate to enable computational sensitivity and uncertainty analyses. We defined a relative error measure to quantify the deformation of the laminate from an ideal paraboloid shape. Using OAT and LHS scheme we have identified the sensitive and significant parameters of the model. Via uncertainty propagation analysis, we found an unexpected bimodal behavior in the RSE distribution under parameter uncertainty. Our investigation of the two modes via Zernike decomposition revealed that astigmatism characterized their difference. We have performed optimization under uncertainty for this model for two different scenarios, and identified nominal values for six important parameters that would produce a better RSE distribution under manufacturer specified uncertainty of the design parameters. Moreover, we have recommended the modification of the tolerance level of parameters to achieve an improved RSE distribution. Optimization obtained with `fminsearch` and CDE algorithms indicate that more advanced methods can be incorporated to find the optimum design parameters for a desired shape or shape error characteristics.

ACKNOWLEDGMENTS

The authors are grateful to the Statistical and Applied Mathematical Sciences Institute (SAMSI). This work was done at the Industrial Mathematical and Statistical Modeling (IMSM) workshop arranged by SAMSI at North Carolina State University in 2017.[10] Sandia National Laboratories is a multimission laboratory managed and operated by National Technology and Engineering Solutions of Sandia LLC, a wholly owned subsidiary of Honeywell International Inc. for the U.S. Department of Energy under contract DE-NA0003525.

REFERENCES

[1] Sumali, H., Massad, J. E., Reu, P. L., Chaplya, P. M., and Martin, J. W., "Analytical and experimental studies of orthotropic corner-supported plates with segmented in-plane actuators," in [*2005 ASME International Mechanical Engineering Congress and Exposition*], 197–202 (2005).

[2] Sumali, H., Massad, J. E., Chaplya, P. M., and Martin, J. W., "Deflection control of a corner-supported plate using segmented in-plane actuators," in [*Proc. ASME IMECE*], **61141** (2004).

[3] Massad, J. E., Washington, G. N., and Sumali, H., "Orthotropic deflection model for corner-supported plates with segmented in-plane actuators," in [*Smart Structures and Materials*], 503–514, International Society for Optics and Photonics (2005).

[4] Reed, R. E., "Comparison of methods in calculating frequencies of corner-supported rectangular plates," in [*NASA Technical Report, NASA-TN-D-3030*], (1965).

[5] Kim, C. and Shannon, R., "Catalog of zernike polynomials," *Applied Optics and Optical Engineering* **10**, 193–221 (1987).

[6] Saltelli, A. and Marivoet, J., "Non-parametric statistics in sensitivity analysis for model output: a comparison of selected techniques," *Reliability Engineering & System Safety* **28**(2), 229–253 (1990).

[7] Iman, R. L., "Latin hypercube sampling," *Encyclopedia of quantitative risk analysis and assessment* (2008).

[8] Price, K. V., "Differential evolution: a fast and simple numerical optimizer," in [*Fuzzy Information Processing Society, 1996. NAFIPS., 1996 Biennial Conference of the North American*], 524–527, IEEE (1996).

[9] Storn, R. and Price, K., "Minimizing the real functions of the ICEC'96 contest by differential evolution," in [*Evolutionary Computation, 1996., Proceedings of IEEE International Conference on*], 842–844, IEEE (1996).

[10] Haider, M., Ipsen, I., Smith, R., and Gremaud, P., "Twenty-third mathematical and statistical modeling workshop for graduate students (crsc-tr17-19),"